Robotica: (2021) volume 39, pp. 1642–1653. © The Author(s), 2021. Published by Cambridge University Press.
doi:10.1017/S0263574720001411

# Effects of Dynamic Model Errors in Task-Priority Operational Space Control

Paolo Di Lillo†*, Gianluca Antonelli† and Ciro Natale‡

†*Department of Electrical and Information Engineering, University of Cassino and Southern Lazio, Cassino, Italy. E-mail: antonelli@unicas.it*
‡*Dipartimento di Ingegneria, Università degli Studi della Campania "Luigi Vanvitelli", Aversa, Italy. E-mail: ciro.natale@unicampania.it*

(Accepted December 14, 2020. First published online: February 1, 2021)

**SUMMARY**
Control algorithms of many Degrees-of-Freedom (DOFs) systems based on Inverse Kinematics (IK) or Inverse Dynamics (ID) approaches are two well-known topics of research in robotics. The large number of DOFs allows the design of many concurrent tasks arranged in priorities, that can be solved either at kinematic or dynamic level. This paper investigates the effects of modeling errors in operational space control algorithms with respect to uncertainties affecting knowledge of the dynamic parameters. The effects on the null-space projections and the sources of steady-state errors are investigated. Numerical simulations with on-purpose injected errors are used to validate the thoughts.

KEYWORDS: Task-priority control; Operational space control; Model uncertainties.

## 1. Introduction

The use of robotic structures with a large number of Degrees-of-Freedom (DOFs) is nowadays common in applications such as humanoids or aerial and underwater robots. Among the various approaches used to control all the DOFs, a popular one is to design several control variables and to arrange them in priority, in a sense that will be clarified later. Within the task-priority approach two frameworks are possible, the Inverse Kinematics (IK) or the Inverse Dynamics (ID). The former commands the robot at position or velocity level, while the latter at torque level.

This paper discusses the modeling errors analysis of operational space control algorithms, belonging to the ID category, with respect to an uncertain knowledge of the dynamic parameters of the mathematical model.

Due to the use of the dynamically consistent pseudoinverse of the Jacobian matrix within the control law, in fact, all the dynamic parameters, including the inertial ones, potentially affect the steady state. In this paper, it will be shown that the steady-state error is influenced only by the errors in the dry friction, the gravity terms compensation, that is, the first moment of inertia, and the possible conflict among the tasks but not by the error in the estimation of the inertial parameters as long as the mass matrix is positive definite.

The validity of the statement has been shown analytically and extensively tested via numerical simulations by varying the number and kind of tasks while resorting to models characterized by various modeling errors. In this paper, a 7DOF robot in nine case studies, with compatible and conflicting tasks, is used as testbed.

The next section discusses the relevant literature, Section 3 provides the necessary mathematical background, Section 4 discusses modeling error issues followed by numerical analysis and finally by the Conclusions.

This paper is a revised version of ref. [2] taking into account the received comments, with a totally revised Section 4 and a new numerical case study. In particular, the main claim of the present paper

* Corresponding author. E-mail: pa.dilillo@unicas.it

remains the same, but it is now better justified as the present paper clarifies how uncertainties affecting the inertia matrix can affect steady-state errors on the primary task even in case of conflicting secondary task only in presence of uncertainties affecting gravity-related terms. Nevertheless, when dynamic errors are relevant, for example, in case of impedance control as primary task, uncertainties on the inertia matrix do affect the desired dynamic behavior but the desired stiffness is always correctly achieved and not influenced by the behavior of the secondary task, conflicting or not.

## 2. Literature Survey

In ref. [7], the operational space approach was first presented to the community. Starting from that seminal input, during the years, a huge research activity has been conducted up to its application to humanoids.[18–20] In ref. [15], several task-priority control laws are presented within a unified approach. The authors show that they all minimize a proper index. The paper also shows an experimental comparison among various techniques in which the resolved rate appears to exhibit superior performances. This has been interpreted as a possible effect of the uncertainty in the knowledge of the dynamic parameters; in detail, it is noticed that this might be amplified by the inversion of the inertia matrix.

In refs. [12, 13], an interesting theoretical and experimental comparison among various kinds of task space control with redundancy resolution is presented. Resolution at velocity, acceleration and torque level is considered for control problems where the primary task is always the end-effector pose while the secondary is the optimization of a proper functional. In the numerical simulation, under ideal conditions, all the controllers exhibited the same performance (*"in numerical simulation, all controllers achieved the same excellent performance,..."*). The following experimental differences are to be ascribed to the unmodelled dynamics, the uncertainty in the model knowledge, the sensor noise and quantization. In particular, the authors notice that acceleration and torque based control requires accurate knowledge of the inertia matrix in order to achieve task decoupling; even if an accurate modeling and identification procedure were implemented, the secondary and primary tasks were coupled. The results reported in the present paper allow to better refine the understanding of this, showing how the uncertainties on the inertia matrix used as weight in the pseudoinverse of the tasks Jacobian matrices do not couple tasks with a different priority. Moreover, the authors refer to several cases of instability that, for the acceleration-based control laws, were ascribed to the difficulty of finding *"a tradeoff between filtering of numeric derivative and choosing higher gain parameters"*. However, the instability problems found by the authors could have been also related to the finite sampling time (unfortunately not reported in the paper) of the digital control implementation and, for the velocity-based controllers, to the use of actual joint states in the computation of joint references $\dot{\boldsymbol{q}}_r$ in the velocity-based controllers. In fact, when actual joint states are used to compute task space errors, then the dynamics of the inner velocity loops play a key role in the stability of the overall system. Both issues, discrete-time implementation and nonideal dynamics of joint velocity loops, are discussed in detail in refs. [3 and 4], where limits to the task space gain are explicitly found related to both sampling time and bandwidth of inner motion control loops.

One of the few papers with an experimental implementation of multiple tasks at dynamic level and their corresponding error representation is provided by ref. [14] where three tasks are arranged in priority, namely the end-effector position, the orientation and the joint configuration. The experiments show steady-state errors for both the first and second priority tasks, which have been explained by the authors as caused by the presence of dry friction and uncertainty in the dynamic knowledge due to the absence of any integral action in their controller. Multiple-task-priority is addressed also in refs. [9, 17].

In ref. [14], the asymptotic stability for an arbitrary number of priority tasks for the particular case of compliance control has been proven. Later, in ref. [6], a formal proof of asymptotic stability for the regulation case of a passivity-based task-priority ID controller is provided making use of the conditional stability theory. Stability of the self-motions has also been studied in refs. [16, 21] in the context of whole-body compliant control of wheeled humanoid robots.

One crucial control aspect is the interaction control. Techniques based on ID may be relatively easily adapted to implement impedance control. In the latter, the design focuses the objective in assigning a desired second-order dynamic behavior with respect to the external force. Access to the joint torques is needed to implement such an approach. In absence of that feature, that is, when

https://doi.org/10.1017/S0263574720001411 Published online by Cambridge University Press

the joints are position or velocity-controlled, one can implement an interaction control defined as admittance or position-based impedance control. An interesting comparison between impedance and admittance control schemes is made in ref. [24]. The strong dependency of the impedance control from the model knowledge is stressed. On the other hand, the admittance control relies on the use of a wrench sensor and, when the interaction is not detected, the controller does not behave with the assigned interaction dynamics but with the low-level one, typically characterized by a larger bandwidth and, in turn, by small compliance to external forces. In the 1-DOF case of impedance control, it is recognized that the sensitivity from the model knowledge increases with a low desired bandwidth. The latter case, that is, a *soft* interaction with the environment or the operator, is thus critical in both the schemes for different reasons. It is worth noticing that, in ref. [24], the comparison is made adopting a model-based controller also for the low-level loop which is not strictly needed.

## 3. Background

### *3.1. Joint-space dynamics*

Equations of motion for serial-chain rigid-body dynamic systems can be written in matrix form as ref. [22]

$$\boldsymbol{M}(\boldsymbol{q})\ddot{\boldsymbol{q}} + \boldsymbol{C}(\boldsymbol{q}, \dot{\boldsymbol{q}})\dot{\boldsymbol{q}} + \boldsymbol{g}(\boldsymbol{q}) = \boldsymbol{\tau}. \tag{1}$$

Denoting with $n$ the number of joints, $\boldsymbol{q} \in \mathbb{R}^n$ is the joint position vector, the *dot* operator represents the time derivative, thus, $\dot{\boldsymbol{q}} \in \mathbb{R}^n$ and $\ddot{\boldsymbol{q}} \in \mathbb{R}^n$ are the vectors of joint velocities and accelerations, respectively, $\boldsymbol{\tau} \in \mathbb{R}^n$ is the joint torque vector, $\boldsymbol{M}(\boldsymbol{q}) \in \mathbb{R}^{n\times n}$ is the inertia matrix, $\boldsymbol{C}(\boldsymbol{q}, \dot{\boldsymbol{q}})\dot{\boldsymbol{q}} \in \mathbb{R}^n$ is the Coriolis and centripetal torque vector and $\boldsymbol{g}(\boldsymbol{q}) \in \mathbb{R}^n$ is the gravity torque vector. By posing

$$\boldsymbol{n}(\boldsymbol{q}, \dot{\boldsymbol{q}}) = \boldsymbol{C}(\boldsymbol{q}, \dot{\boldsymbol{q}})\dot{\boldsymbol{q}} + \boldsymbol{g}(\boldsymbol{q}), \tag{2}$$

Eq. (1) is often presented in the more compact form as

$$\boldsymbol{M}(\boldsymbol{q})\ddot{\boldsymbol{q}} + \boldsymbol{n}(\boldsymbol{q}, \dot{\boldsymbol{q}}) = \boldsymbol{\tau}. \tag{3}$$

### *3.2. Task-space dynamics*

The control objective is often the position and orientation of the end effector; however, in advanced robotics and with many DOFs available, several other tasks can be defined. It is then possible to introduce a generic task as

$$\boldsymbol{\sigma}_x = \boldsymbol{\sigma}(\boldsymbol{q}), \tag{4}$$

with $\boldsymbol{\sigma}_x \in \mathbb{R}^{m_x}$ the task function. It holds

$$\dot{\boldsymbol{\sigma}}_x = \boldsymbol{J}_x(\boldsymbol{q})\dot{\boldsymbol{q}}, \tag{5}$$

$$\ddot{\boldsymbol{\sigma}}_x = \boldsymbol{J}_x(\boldsymbol{q})\ddot{\boldsymbol{q}} + \dot{\boldsymbol{J}}_x(\boldsymbol{q}, \dot{\boldsymbol{q}})\dot{\boldsymbol{q}} \tag{6}$$

in which the matrix $\boldsymbol{J}_x(\boldsymbol{q}) \in \mathbb{R}^{m_x\times n}$ is lower rectangular, that is, with more columns than rows.

Let us recall the equations of motion in the task space. It holds

$$\boldsymbol{\tau} = \boldsymbol{J}_x^T(\boldsymbol{q})\boldsymbol{f}_x, \tag{7}$$

where $\boldsymbol{f}_x \in \mathbb{R}^{m_x}$ is the task *generalized* force vector. The joint accelerations can then be found as

$$\ddot{\boldsymbol{q}} = \boldsymbol{M}^{-1}(\boldsymbol{q})\left[\boldsymbol{J}_x^T(\boldsymbol{q})\boldsymbol{f}_x - \boldsymbol{n}(\boldsymbol{q}, \dot{\boldsymbol{q}})\right], \tag{8}$$

that, substituted in (6), gives

$$\begin{aligned}\ddot{\boldsymbol{\sigma}}_x = {} & \boldsymbol{J}_x(\boldsymbol{q})\boldsymbol{M}^{-1}(\boldsymbol{q})\boldsymbol{J}_x^T(\boldsymbol{q})\boldsymbol{f}_x + \\ & -\boldsymbol{J}_x(\boldsymbol{q})\boldsymbol{M}^{-1}(\boldsymbol{q})\boldsymbol{n}(\boldsymbol{q}, \dot{\boldsymbol{q}}) + \dot{\boldsymbol{J}}_x(\boldsymbol{q}, \dot{\boldsymbol{q}})\dot{\boldsymbol{q}}.\end{aligned} \tag{9}$$

By defining

$$\boldsymbol{M}_x(\boldsymbol{q}) = \left(\boldsymbol{J}_x(\boldsymbol{q})\boldsymbol{M}^{-1}(\boldsymbol{q})\boldsymbol{J}_x^T(\boldsymbol{q})\right)^{-1} \in \mathbb{R}^{m_x\times m_x} \tag{10}$$

https://doi.org/10.1017/S0263574720001411 Published online by Cambridge University Press

and

$$\boldsymbol{c}_x(\boldsymbol{q}, \dot{\boldsymbol{q}}) = \boldsymbol{M}_x(\boldsymbol{q}) \left( \boldsymbol{J}_x(\boldsymbol{q}) \boldsymbol{M}^{-1}(\boldsymbol{q}) \boldsymbol{C}(\boldsymbol{q}, \dot{\boldsymbol{q}}) \dot{\boldsymbol{q}} - \dot{\boldsymbol{J}}_x(\boldsymbol{q}, \dot{\boldsymbol{q}}) \dot{\boldsymbol{q}} \right)$$
$$\boldsymbol{g}_x(\boldsymbol{q}) = \boldsymbol{M}_x(\boldsymbol{q}) \boldsymbol{J}_x(\boldsymbol{q}) \boldsymbol{M}^{-1}(\boldsymbol{q}) \boldsymbol{g}(\boldsymbol{q})$$

the task space dynamics is described by

$$\boldsymbol{M}_x(\boldsymbol{q}) \ddot{\boldsymbol{\sigma}}_x + \boldsymbol{c}_x(\boldsymbol{q}, \dot{\boldsymbol{q}}) + \boldsymbol{g}_x(\boldsymbol{q}) = \boldsymbol{f}_x. \tag{11}$$

Let us further define

$$\begin{aligned} \overline{\boldsymbol{J}}_x(\boldsymbol{q}) &= \boldsymbol{M}^{-1}(\boldsymbol{q}) \boldsymbol{J}_x^T(\boldsymbol{q}) \boldsymbol{M}_x(\boldsymbol{q}) \\ &= \boldsymbol{M}^{-1}(\boldsymbol{q}) \boldsymbol{J}_x^T(\boldsymbol{q}) \left( \boldsymbol{J}_x(\boldsymbol{q}) \boldsymbol{M}^{-1}(\boldsymbol{q}) \boldsymbol{J}_x^T(\boldsymbol{q}) \right)^{-1} \in \mathbb{R}^{n \times m_x}, \end{aligned} \tag{12}$$

that is, the weighted pseudoinverse where the weight is the inverse of the inertia matrix. This is defined as the dynamically consistent pseudoinverse.[7] It holds

$$\boldsymbol{J}_x(\boldsymbol{q}) \overline{\boldsymbol{J}}_x(\boldsymbol{q}) = \boldsymbol{I}_{m_x}. \tag{13}$$

The relationship (7) is invertible in

$$\boldsymbol{f}_x = \overline{\boldsymbol{J}}_x^T(\boldsymbol{q}) \boldsymbol{\tau}, \tag{14}$$

where, being $n > m_x$, the null space of $\overline{\boldsymbol{J}}_x^T(\boldsymbol{q})$ needs to be taken into account and a more general joint torque $\boldsymbol{\tau}$ corresponding to the task space force $\boldsymbol{f}_x$ is

$$\boldsymbol{\tau} = \boldsymbol{J}_x^T(\boldsymbol{q}) \boldsymbol{f}_x + \overline{\boldsymbol{N}}_x(\boldsymbol{q}) \boldsymbol{\tau}_0 \tag{15}$$

in which $\boldsymbol{\tau}_0$ is a vector of arbitrary torques and the null-space projector is

$$\overline{\boldsymbol{N}}_x(\boldsymbol{q}) = \boldsymbol{I}_n - \boldsymbol{J}_x^T(\boldsymbol{q}) \overline{\boldsymbol{J}}_x^T(\boldsymbol{q}), \tag{16}$$

that gives

$$\overline{\boldsymbol{J}}_x^T(\boldsymbol{q}) \overline{\boldsymbol{N}}_x = \overline{\boldsymbol{J}}_x^T(\boldsymbol{q}) - \overline{\boldsymbol{J}}_x^T(\boldsymbol{q}) = \boldsymbol{O}_{m_x \times n}. \tag{17}$$

Notice that, due to a different definition of the null-space projector in Eq. (16), part of the literature exhibits a transpose operator in the Eq. (15) and its derivatives. The result is obviously the same.

Remarkably, Eq. (17) holds for any positive-definite weight matrix used to compute $\overline{\boldsymbol{J}}_x^T(\boldsymbol{q})$ in $\overline{\boldsymbol{N}}_x(\boldsymbol{q})$ and, in turn, for inertial parameters affected by uncertainties of any entity as long as the weight matrix is still positive definite.

In the following, dependencies will be omitted to improve readability.

### *3.3. Single-task operational space control*

In ref. [7], the approach known as "operational space control" is proposed. By assuming that the subscript $d$ means "desired", the control objective is to track a desired task trajectory $\boldsymbol{\sigma}_{x,d}(t)$. If the symbol $\tilde{\cdot}$ denotes the error defined by the desired minus the actual value, by choosing

$$\boldsymbol{f}_x = \boldsymbol{M}_x \left( \ddot{\boldsymbol{\sigma}}_{x,d} + \boldsymbol{K}_v \dot{\tilde{\boldsymbol{\sigma}}}_x + \boldsymbol{K}_p \tilde{\boldsymbol{\sigma}}_x \right) + \boldsymbol{c}_x + \boldsymbol{g}_x \tag{18}$$

in Eq. (7), with $\boldsymbol{K}_v > \boldsymbol{O}$ and $\boldsymbol{K}_p > \boldsymbol{O}$ design gains of proper dimensions, one obtains

$$\boldsymbol{M}_x \ddot{\boldsymbol{\sigma}}_x = \boldsymbol{M}_x \left( \ddot{\boldsymbol{\sigma}}_{x,d} + \boldsymbol{K}_v \dot{\tilde{\boldsymbol{\sigma}}}_x + \boldsymbol{K}_p \tilde{\boldsymbol{\sigma}}_x \right) \tag{19}$$

and thus a second-order error dynamics

$$\ddot{\tilde{\boldsymbol{\sigma}}}_x + \boldsymbol{K}_v \dot{\tilde{\boldsymbol{\sigma}}}_x + \boldsymbol{K}_p \tilde{\boldsymbol{\sigma}}_x = \boldsymbol{0}. \tag{20}$$

https://doi.org/10.1017/S0263574720001411 Published online by Cambridge University Press

The controller at torque level is ref. [7]

$$\boldsymbol{\tau} = \boldsymbol{J}_x^T \boldsymbol{M}_x \left( \ddot{\boldsymbol{\sigma}}_{x,d} + \boldsymbol{K}_v \dot{\tilde{\boldsymbol{\sigma}}}_x + \boldsymbol{K}_p \tilde{\boldsymbol{\sigma}}_x \right) + \boldsymbol{c}'_x + \boldsymbol{g}'_x, \tag{21}$$

in which $\boldsymbol{g}'_x$ embeds gravity and the term $\boldsymbol{c}'_x$ embeds the velocity terms. A damping term in the joint and task spaces are then necessary for the redundant case to achieve asymptotic stability.[7]

It is worth noticing that also the compensation of the Coriolis and centripetal and gravity terms, that is, the vector $\boldsymbol{n}(\boldsymbol{q}, \dot{\boldsymbol{q}})$ in Eq. (3), may be also achieved more simply at torque level.[12,22]

### *3.4. Task-priority operational space control*

In case of two tasks denoted as $a$ and $b$, the applied torque is refs. [18, 19]

$$\boldsymbol{\tau} = \boldsymbol{\tau}_a + \overline{\boldsymbol{N}}_a \boldsymbol{\tau}_b, \tag{22}$$

where both $\boldsymbol{\tau}_a$ and $\boldsymbol{\tau}_b$ are given by (21) properly modifying the subscripts and the null-space projector is given by (16).

To better appreciate the control laws, it is useful to rewrite the task dynamics of the generic task $x$ by properly projecting it as

$$\overline{\boldsymbol{J}}_x^T \left[ \boldsymbol{M}\ddot{\boldsymbol{q}} + \boldsymbol{n} = \boldsymbol{\tau} \right], \tag{23}$$

which implies

$$\boldsymbol{M}_x \ddot{\boldsymbol{\sigma}}_x + \boldsymbol{c}_x + \boldsymbol{g}_x = \overline{\boldsymbol{J}}_x^T \boldsymbol{\tau}. \tag{24}$$

In the $a$ task, thus, the dynamics is described by

$$\boldsymbol{M}_a \ddot{\boldsymbol{\sigma}}_a + \boldsymbol{c}_a + \boldsymbol{g}_a = \overline{\boldsymbol{J}}_a^T \boldsymbol{\tau}_a \tag{25}$$

while in the $b$ task by

$$\boldsymbol{M}_b \ddot{\boldsymbol{\sigma}}_b + \boldsymbol{c}_b + \boldsymbol{g}_b = \overline{\boldsymbol{J}}_b^T \left( \boldsymbol{\tau}_a + \overline{\boldsymbol{N}}_a \boldsymbol{\tau}_b \right). \tag{26}$$

Extensions to $n$ tasks can be found in ref. [19].

The work[15] proposes a formulation for redundant robots for several control laws. For two tasks the expression sounds like

$$\boldsymbol{\tau} = \boldsymbol{\tau}_b + \boldsymbol{\tau}_a(\boldsymbol{\tau}_b) \tag{27}$$

in which $\boldsymbol{\tau}_b$ is the action of the lower priority task and the higher priority ones are achieved by *canceling* the lower priority ones.

Other task-priority ID-based approaches have been proposed in, for example, refs. [9, 17].

### *3.5. Stability analysis*

While the stability of the primary task is deeply discussed for all the techniques above, the same is not true for the lower priority tasks, even for a simple two-task case. As noticed in, for example, refs. [12, 13], until recently no analytic discussion existed. The stability of all the tasks for a generic number of them and for four different velocity-based IK algorithms has been solved in refs. [1, 11], but only at kinematic level. In ref. [10], it has been extended to the set-based case with the constraint that the set-based tasks need to stay at higher priority levels.

In ref. [8], the lower priority task Jacobians are modified as, limiting to the second task for consistency within this document,

$$\boldsymbol{J}_{b|a} = \boldsymbol{J}_b \overline{\boldsymbol{N}}_a^T$$

and defined as *task-consistent secondary Jacobian* (as remarked above, due to the definitions of the variables, here the transpose of the null-space projector matrix is reversed with respect to the original paper). The authors also define a proper task-consistent secondary matrix as

$$\boldsymbol{M}_{b|a}(\boldsymbol{q}) = \left( \boldsymbol{J}_{b|a}(\boldsymbol{q}) \boldsymbol{M}^{-1}(\boldsymbol{q}) \boldsymbol{J}_{b|a}^T(\boldsymbol{q}) \right)^{-1} \in \mathbb{R}^{m_b \times m_b}.$$

https://doi.org/10.1017/S0263574720001411 Published online by Cambridge University Press

In order to understand what happens in the $b$ task space, the projection similar to Eq. (23) is then obtained by resorting to the matrix $\overline{\boldsymbol{J}}_{b|a}^T$. In ref. [18], there are some reasonable considerations on the task functions and some textual descriptions of convergence *"within the corresponding null space"*.

The authors of ref. [15], even though they propose a nice unifying framework for control of redundant robots, they clearly admit that *"the stability of this framework as most related approaches derivable from this framework cannot be shown conclusively but only in special cases"*. They provide only necessary conditions for stability and prove that the hierarchical composition method of multiple tasks does not generate conflicts among tasks at different priorities.

Only recently the first stability results for the task-priority ID approaches appeared in the literature for particular cases. In ref. [14], stability has been proven for compliance control. In the latter approach, the limit is that it is not possible to assign the desired inertia but the system will keep its natural one. A formal proof of asymptotic stability of a passivity-based task-priority ID controller is provided in ref. [6] for the regulation case and in ref. [5] for the tracking case, making use of the conditional stability theory. The analysis does not require that the tasks are compatible, that is, their corresponding augmented Jacobian may be not-full-rank.

In ref. [17], multi-priority control is addressed at the acceleration level. The authors, moreover, further show that the lower priority tasks do not affect the higher priority ones, regardless the weight matrix used in the pseudoinverse computation, that is, also when using the dynamically consistent one. This result extends their stability analysis to the inverse dynamics case and provides a clue on the sensitivity considerations made.

## 4. Modeling Error Analysis

The ID task-priority algorithm implemented in this paper is inspired by the one in Eq. (22) with control torques for tasks $a$ and $b$ as in Eq. (21), and here explicitly reported by compensating the nonlinear dynamics directly in the joint space

$$\begin{aligned}\boldsymbol{\tau} = &\underbrace{\boldsymbol{J}_a^T\hat{\boldsymbol{M}}_a\left(\ddot{\boldsymbol{\sigma}}_{a,d} + \boldsymbol{K}_{a,v}\dot{\tilde{\boldsymbol{\sigma}}}_a + \boldsymbol{K}_{a,p}\tilde{\boldsymbol{\sigma}}_a - \dot{\boldsymbol{J}}_a\dot{\boldsymbol{q}}\right)}_{\boldsymbol{\tau}_a} \\ &+ \hat{\overline{\boldsymbol{N}}}_a\underbrace{\boldsymbol{J}_b^T\hat{\boldsymbol{M}}_b\left(\ddot{\boldsymbol{\sigma}}_{b,d} + \boldsymbol{K}_{b,v}\dot{\tilde{\boldsymbol{\sigma}}}_b + \boldsymbol{K}_{b,p}\tilde{\boldsymbol{\sigma}}_b - \dot{\boldsymbol{J}}_b\dot{\boldsymbol{q}}\right)}_{\boldsymbol{\tau}_b} + \hat{\boldsymbol{n}},\end{aligned} \tag{28}$$

where all the matrices depending on the dynamic parameters are considered uncertain, hence denoted with the symbol $\hat{\cdot}$, and the matrices depending on the sole kinematic parameters are considered perfectly known. Notice that the latter assumption reflects the state of the art in modeling knowledge, that is, kinematic parameters are known with accuracy order of magnitudes larger than dynamic ones.

In order to understand the dynamics in the higher priority task we re-project (28) according to $\hat{\overline{\boldsymbol{J}}}_a^T$ yielding

$$\hat{\overline{\boldsymbol{J}}}_a^T\boldsymbol{M}\ddot{\boldsymbol{q}} + \hat{\overline{\boldsymbol{J}}}_a^T\boldsymbol{n} = \hat{\overline{\boldsymbol{J}}}_a^T\boldsymbol{J}_a^T\hat{\boldsymbol{M}}_a\ddot{\boldsymbol{\sigma}}_{a,r} + \hat{\overline{\boldsymbol{J}}}_a^T\hat{\overline{\boldsymbol{N}}}_a\boldsymbol{\tau}_b + \hat{\overline{\boldsymbol{J}}}_a^T\hat{\boldsymbol{n}},$$

where the definition of $\ddot{\boldsymbol{\sigma}}_{a,r}$

$$\ddot{\boldsymbol{\sigma}}_{a,r} = \ddot{\boldsymbol{\sigma}}_{a,d} + \boldsymbol{K}_{a,v}\dot{\tilde{\boldsymbol{\sigma}}}_a + \boldsymbol{K}_{a,p}\tilde{\boldsymbol{\sigma}}_a - \dot{\boldsymbol{J}}_a\dot{\boldsymbol{q}}$$

helps in the equation reading.

Interestingly, the term $\hat{\overline{\boldsymbol{J}}}_a^T\hat{\overline{\boldsymbol{N}}}_a\boldsymbol{\tau}_b$ disappears due to the specific projection selected. Moreover, given $\hat{\overline{\boldsymbol{J}}}_a^T\boldsymbol{J}_a^T = \boldsymbol{I}$ and exploiting the definition of the various terms yields

$$\left(\boldsymbol{J}_a\hat{\boldsymbol{M}}^{-1}\boldsymbol{J}_a^T\right)^{-1}\boldsymbol{J}_a\hat{\boldsymbol{M}}^{-1}\boldsymbol{M}\ddot{\boldsymbol{q}} = \hat{\boldsymbol{M}}_a\ddot{\boldsymbol{\sigma}}_{a,r} + \hat{\overline{\boldsymbol{J}}}_a^T\tilde{\boldsymbol{n}},$$

being $\tilde{\boldsymbol{n}} = \hat{\boldsymbol{n}} - \boldsymbol{n}$, that is

$$\hat{\boldsymbol{M}}_a\boldsymbol{J}_a\hat{\boldsymbol{M}}^{-1}\boldsymbol{M}\ddot{\boldsymbol{q}} = \hat{\boldsymbol{M}}_a\ddot{\boldsymbol{\sigma}}_{a,r} + \hat{\overline{\boldsymbol{J}}}_a^T\tilde{\boldsymbol{n}},$$

https://doi.org/10.1017/S0263574720001411 Published online by Cambridge University Press

which can be rewritten as

$$\boldsymbol{J}_a\ddot{\boldsymbol{q}} - \boldsymbol{J}_a\ddot{\boldsymbol{q}} + \boldsymbol{J}_a\hat{\boldsymbol{M}}^{-1}\boldsymbol{M}\ddot{\boldsymbol{q}} = \ddot{\boldsymbol{\sigma}}_{a,r} + \hat{\boldsymbol{M}}_a^{-1}\hat{\boldsymbol{J}}_a^T\tilde{\boldsymbol{n}}$$

and finally, in view of (6), the sought equation

$$\ddot{\tilde{\boldsymbol{\sigma}}}_a + \boldsymbol{K}_{a,v}\dot{\tilde{\boldsymbol{\sigma}}}_a + \boldsymbol{K}_{a,p}\tilde{\boldsymbol{\sigma}}_a = \underbrace{\boldsymbol{J}_a\left(\hat{\boldsymbol{M}}^{-1}\boldsymbol{M} - \boldsymbol{I}\right)\ddot{\boldsymbol{q}} + \boldsymbol{J}_a\hat{\boldsymbol{M}}^{-1}\tilde{\boldsymbol{n}}}_{\boldsymbol{\varphi}}. \tag{29}$$

The *disturbance* term is state-dependent, that is, $\boldsymbol{\varphi} = \boldsymbol{\varphi}(\boldsymbol{q}, \dot{\boldsymbol{q}}, \ddot{\boldsymbol{q}})$ and vanishes for perfect compensation.

The modeling errors, thus, do not affect the projections from lower to higher priority tasks. They act with two configuration-dependent terms, one function also of the joint accelerations and the other of the joint velocities.

With the further assumption that the system reaches a steady-state, that is, $\ddot{\boldsymbol{q}} = \boldsymbol{0}$, $\dot{\boldsymbol{q}} = \boldsymbol{0}$, the additional comment that can be done is that a steady-state error in the task space $a$ is caused by a wrong gravity compensation since Eq. (29) becomes

$$\tilde{\boldsymbol{\sigma}}_a = \boldsymbol{K}_{a,p}^{-1}\boldsymbol{J}_a\hat{\boldsymbol{M}}^{-1}\tilde{\boldsymbol{g}}. \tag{30}$$

The above conclusion, however, does not take into account another important dynamic effect, commonly ignored in the stability analysis of robot control, the dry friction. The latter is a phenomenon affecting low/null velocities hard to model and, consequently, to compensate for. From the mathematical perspective, with certain confidence under the assumptions made, it can be considered as embed in the error of gravity compensation, that is, a configuration-dependent term not vanishing at steady state. The conclusion is thus that modeling errors do not distort the projections as long as the mass still is positive definite while, however, they obviously affect the transient. It seems that the steady-state experimental errors remarked, for example, in refs. [12–14] are thus to be attributed, beyond the digitization issues discussed, to the gravity and friction compensation terms. Nevertheless, the uncertainty of gravity torque is not the only source of steady-state task error, in fact, Eq. (30) clearly shows how such error is affected by the estimated inertia matrix. In detail, given the uncertainty on the gravity torque, the steady-state error can be different in case of different uncertainties affecting the inertia matrix, as it will be shown in Section 5.

This aspect is even more relevant taking into account that the modeling errors affecting the inertia matrix and the gravity-related terms are identified usually with a different *accuracy* for two reasons. The first reason is due to the fact that the dynamic parameters affecting the mass matrix are the link masses and inertia while the dynamic parameters affecting the gravity are the first moment of inertia, that is, the center of gravity of the links multiplied by the masses. The two different class of terms, being excited during the experiments by joint accelerations and positions respectively, are differently affected by the corresponding *quality* of the data. The joint accelerations being noisier with respect to the joint positions (in most of the cases accelerations are obtained from positions by filtering and numerical differentiation) it results that the inertia-related dynamic parameters exhibit an uncertainty that is larger than the gravity-related ones. In addition to that, the various identification techniques output models with different properties. Surprisingly enough, most of the techniques do not guarantee a positive-definite joint-space inertia matrix.[23]

In refs. [12, 13], the secondary task is an optimization achieved via a gradient operation of a proper functional. This means that the secondary task control input is always non-null, except in a local minimum, and thus it always projects a value on the null space of the higher priority task. This case will be numerically simulated in the next section by defining a secondary task in conflict with the primary one reaching, thus, a non-null steady-state error. The considerations above remain confirmed.

## 5. Numerical Case Studies

In this section, the theoretical results shown in Section 4 are validated via numerical dynamic simulations of the operational space control law in Eq. (28), which have been run by considering a KUKA

https://doi.org/10.1017/S0263574720001411 Published online by Cambridge University Press

Table I. Steady-state errors for different uncertainty amplitudes in $\boldsymbol{M}(\boldsymbol{q})$.

| **Uncertainty in $\boldsymbol{g}(\boldsymbol{q})$ (%)** | **Uncertainty in $\boldsymbol{M}(\boldsymbol{q})$ (%)** | **Steady-state task error norm (cm)** |
|---|---|---|
| 50 | 10 | 0.77 |
| 50 | 20 | 0.87 |
| 50 | 30 | 0.99 |
| 50 | 40 | 1.14 |
| 50 | 50 | 1.35 |

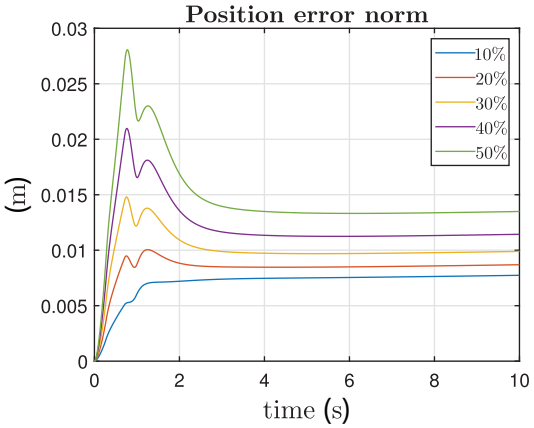


Fig. 1. Results of the first simulations. The steady-state task error norm grows together with the uncertainty on the inertia-related terms when a fixed 50% uncertainty affects the gravity term.

LBR III. We have chosen to perform simulations because no experiments would have confirmed the achieved results due to the absence of the ground truth with experimental data.

Before analyzing the case studies in Table II, we have carried out a specific simulation to show the effects of uncertainties affecting both gravity and inertia-related terms on the steady-state error as computed in Eq. (30).

Uncertainties on the gravity term have been modeled as a percentage error on the position of the center of gravity of the links with respect to the nominal values, while uncertainties on the inertia-related terms are a percentage error affecting link masses, the center of gravity positions as well as inertia tensors. In particular, the uncertainty on the gravity term is fixed at 50%, while uncertainty on the inertia-related terms varies from 10% to 50%, resulting in five simulations. The task taken into account is

$$\boldsymbol{\sigma} = \boldsymbol{p}_e(\boldsymbol{q}) \in \mathbb{R}^3,$$

where $\boldsymbol{p}_e(\boldsymbol{q})$ is the position of the end-effector with respect to the base frame.

The gains of the operational space control law, digitally implemented with a sampling time of 1 ms, are as follows:

$$\boldsymbol{K}_v = 10\boldsymbol{I}_3,\ \boldsymbol{K}_p = 10\boldsymbol{I}_3.$$

Figure 1 shows the norm of the position error for the five simulations. It is clear that uncertainties on the inertial terms affect both the transient and the steady-state as expected, given the imperfect compensation of the gravity term. In particular, it is possible to notice that the steady-state errors grow together with the uncertainties on the inertial terms, as reported in Table I.

With reference to Table II, the group of numerical simulations in which the inertia matrix $\boldsymbol{M}(\boldsymbol{q})$ is uncertain have been simulated by considering amplitude uncertainty factors of 40% of the nominal value. Moreover, in some case studies, a perfect compensation of the nonlinear terms in Eq. (2) has been assumed so as to leave only the effects of an uncertain inertia matrix. Dry friction is not simulated.

https://doi.org/10.1017/S0263574720001411 Published online by Cambridge University Press

Table II. Table of the case studies investigated in the numerical simulations.

| | **Case study task *a*/task *b*** | **Knowledge of $\boldsymbol{M}(\boldsymbol{q})$** | **Knowledge of $\boldsymbol{g}(\boldsymbol{q})$** |
|---|---|---|---|
| (1) | Tracking/tracking, comp. | Perfect | Perfect |
| (2) | Tracking/tracking, comp. | Uncertain | Perfect |
| (3) | Tracking/tracking, comp. | Uncertain | Uncertain |
| (4) | Tracking/tracking, confl. | Perfect | Perfect |
| (5) | Tracking/tracking, confl. | Uncertain | Perfect |
| (6) | Tracking/tracking, confl. | Uncertain | Uncertain |
| (7) | Impedance/tracking | Perfect | Perfect |
| (8) | Impedance/tracking | Perfect | Uncertain |
| (9) | Impedance/tracking | Uncertain | Uncertain |

The case studies from 1 to 3 concern compatible tasks, in detail,

$(a)$ $\boldsymbol{\sigma}_a = \boldsymbol{p}_e(\boldsymbol{q}) \in \mathbb{R}^3$,
$(b)$ $\boldsymbol{\sigma}_b = \boldsymbol{\varepsilon}_e(\boldsymbol{q}) \in \mathbb{R}^3$,

where $\boldsymbol{\varepsilon}_e(\boldsymbol{q})$ and $\boldsymbol{p}_e(\boldsymbol{q})$ are the vector part of the quaternion and the position vector expressing end-effector orientation and position with respect to the base frame, respectively. The gains of the operational space control law, are as follows:

$$\boldsymbol{K}_{a,v} = 100\boldsymbol{I}_3,\ \boldsymbol{K}_{a,p} = 500\boldsymbol{I}_3,$$
$$\boldsymbol{K}_{b,v} = 100\boldsymbol{I}_3,\ \boldsymbol{K}_{b,p} = 500\boldsymbol{I}_3.$$

The case studies from 4 to 6 concern conflicting tasks. In detail,

$(a)$ $\sigma_a = d_w(\boldsymbol{q}) \in \mathbb{R}$,
$(b)$ $\boldsymbol{\sigma}_b = \boldsymbol{p}_e(\boldsymbol{q}) \in \mathbb{R}^3$,

where $\boldsymbol{p}_e(\boldsymbol{q})$ is the end-effector position and $d_w(\boldsymbol{q})$ is the distance from a vertical virtual wall placed at $-0.5$ m along the $x$-axis of the arm base frame. The reference position for the secondary task has been chosen beyond the virtual wall while the reference distance for the primary task has been set at 10 cm in order to design a case study with conflicting tasks. The gains of the ID control law, are as follows:

$$K_{a,v} = 10,\ K_{a,p} = 50,$$
$$\boldsymbol{K}_{b,v} = 20\boldsymbol{I}_3,\ \boldsymbol{K}_{b,p} = 100\boldsymbol{I}_3.$$

Figure 2 collects the relevant results of the first six case studies.

The three top plots report the task errors for cases 1–3. In the top-left plot, it can be noticed that with a perfect compensation of the dynamics and compatible tasks both the errors nicely converge to zero after the transient. In the second case study, the top-center plot shows that, despite the wrong compensation of the inertial terms, when the nonlinear compensation $\boldsymbol{n}$ is correct both primary and secondary tasks converge to zero. The top-right plot shows that the cause of the steady-state error is due to the wrong compensation of $\boldsymbol{n}$, in particular, the sole persistent term at steady-state, that is, the gravity $\boldsymbol{g}$. Similar plots have been reported in the bottom plots where the task errors of the conflicting case are reported. The task $b$ error is always different from zero at steady-state, as obvious due to the filtering action of the null-space projection. The primary task, however, exhibits null error both for perfect modeling compensation (bottom-left) and uncertainty in the inertia matrix with perfect compensation of the terms $\boldsymbol{n}$ (bottom-center). The primary task, thus, converges despite the uncertainty on the compensation of the inertial terms in $\hat{\overline{\boldsymbol{N}}}_a$ supporting the considerations made in Section 4. The bottom-right plot shows the sole case where there is a steady-state error, that is, when the gravity compensation is wrong.

https://doi.org/10.1017/S0263574720001411 Published online by Cambridge University Press

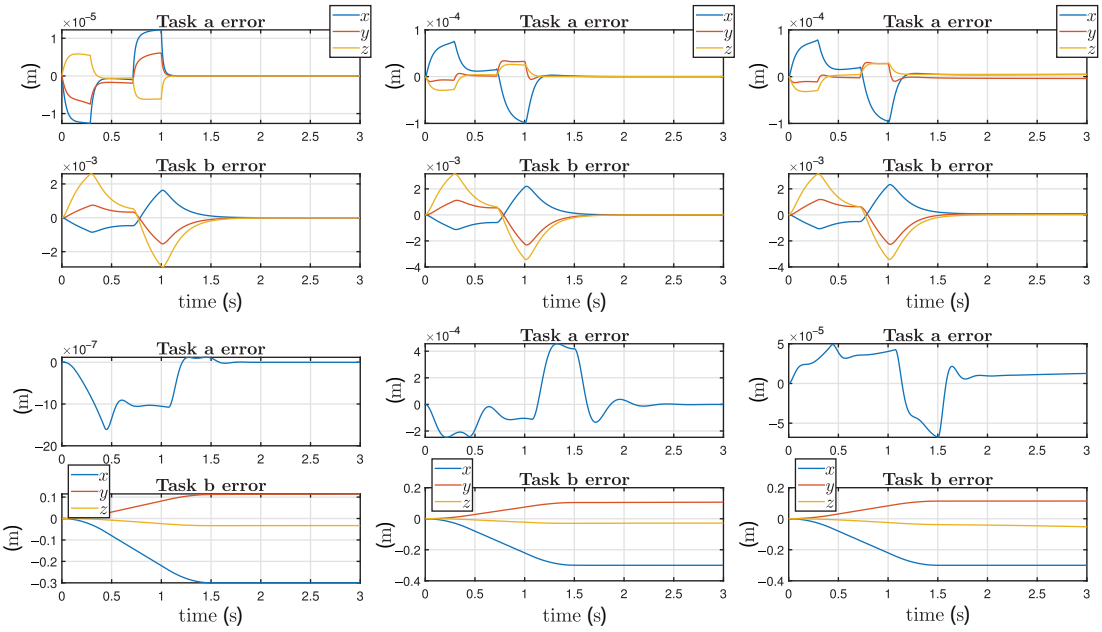


Fig. 2. Case studies 1–6. Top-left: Compatible tasks, perfect compensation of inertial and nonlinear terms. Top-center: Compatible tasks, imperfect knowledge of the inertia matrix. Top-right Compatible tasks, imperfect compensation of both inertial and nonlinear terms. Bottom-left: Conflicting tasks, perfect compensation of inertial and nonlinear terms. Bottom-center Conflicting tasks, imperfect knowledge of the inertia matrix. Bottom-right: Conflicting tasks, imperfect compensation of both inertial and nonlinear terms.

As noticed in ref. [24] and briefly discussed in Section 2, poor knowledge of the dynamic parameters affects the impedance loop. In the following, the control law (28) has been modified to implement an impedance scheme as primary task, that is,

$$\boldsymbol{\tau} = \boldsymbol{J}_a^T \hat{\boldsymbol{M}}_a \ddot{\boldsymbol{\sigma}}_{a,r} + \hat{\bar{\boldsymbol{N}}}_a \boldsymbol{\tau}_b + \hat{\boldsymbol{n}} - \boldsymbol{J}^T \boldsymbol{f}, \tag{31}$$

where $\ddot{\boldsymbol{\sigma}}_{a,r}$ is defined as

$$\ddot{\boldsymbol{\sigma}}_{a,r} = \ddot{\boldsymbol{\sigma}}_{a,d} + \boldsymbol{K}_{a,m}^{-1} \boldsymbol{K}_{a,v} \dot{\tilde{\boldsymbol{\sigma}}}_a + \boldsymbol{K}_{a,m}^{-1} \boldsymbol{K}_{a,p} \tilde{\boldsymbol{\sigma}}_a - \boldsymbol{K}_{a,m}^{-1} \boldsymbol{f}_a - \dot{\boldsymbol{J}}_a \dot{\boldsymbol{q}} \tag{32}$$

being $\boldsymbol{f} \in \mathbb{R}^6$ the end-effector wrench, $\boldsymbol{K}_{a,m} \in \mathbb{R}^{m_a \times m_a}$, $\boldsymbol{K}_{a,v} \in \mathbb{R}^{m_a \times m_a}$, $\boldsymbol{K}_{a,p} \in \mathbb{R}^{m_a \times m_a}$ the mass, damping and stiffness matrices of the desired impedance, $\boldsymbol{f}_a$ the generalized force in the $a$ task space and $\boldsymbol{\tau}_b$ implements a generic secondary task. For the case at hand, the following tasks have been implemented:

(*a*) $\boldsymbol{\sigma}_a = \boldsymbol{p}_e(\boldsymbol{q}) \in \mathbb{R}^3$ ,
(*b*) $\boldsymbol{\sigma}_b = \boldsymbol{q} \in \mathbb{R}^7$.

A point contact is assumed at the end effector such that the contact force $\boldsymbol{f}_a$ is

$$\boldsymbol{f}_a = \boldsymbol{K}_{\text{env}} (\boldsymbol{p}_e(\boldsymbol{q}) - \boldsymbol{p}_0), \tag{33}$$

where $\boldsymbol{p}_0$ is one point representing the equilibrium position of the environment assumed purely elastic with semi-positive definite stiffness matrix $\boldsymbol{K}_{\text{env}}$.

Please notice that this version of the controller considers the perfect compensation of the end-effector contact wrench. Alternative versions without this assumption or with compensation of contact wrenches along the robotic structure may be implemented as well. The control gains have been selected as

$$\boldsymbol{K}_{a,m} = 2\boldsymbol{I}_3 \quad \boldsymbol{K}_{a,v} = 45\boldsymbol{I}_3 \quad \boldsymbol{K}_{a,p} = 60\boldsymbol{I}_3,$$

while the environment stiffness matrix is

$$\boldsymbol{K}_{\text{env}} = \text{diag}\,([30\,0\,0]^T)\ \text{N/m}. \tag{34}$$

https://doi.org/10.1017/S0263574720001411 Published online by Cambridge University Press

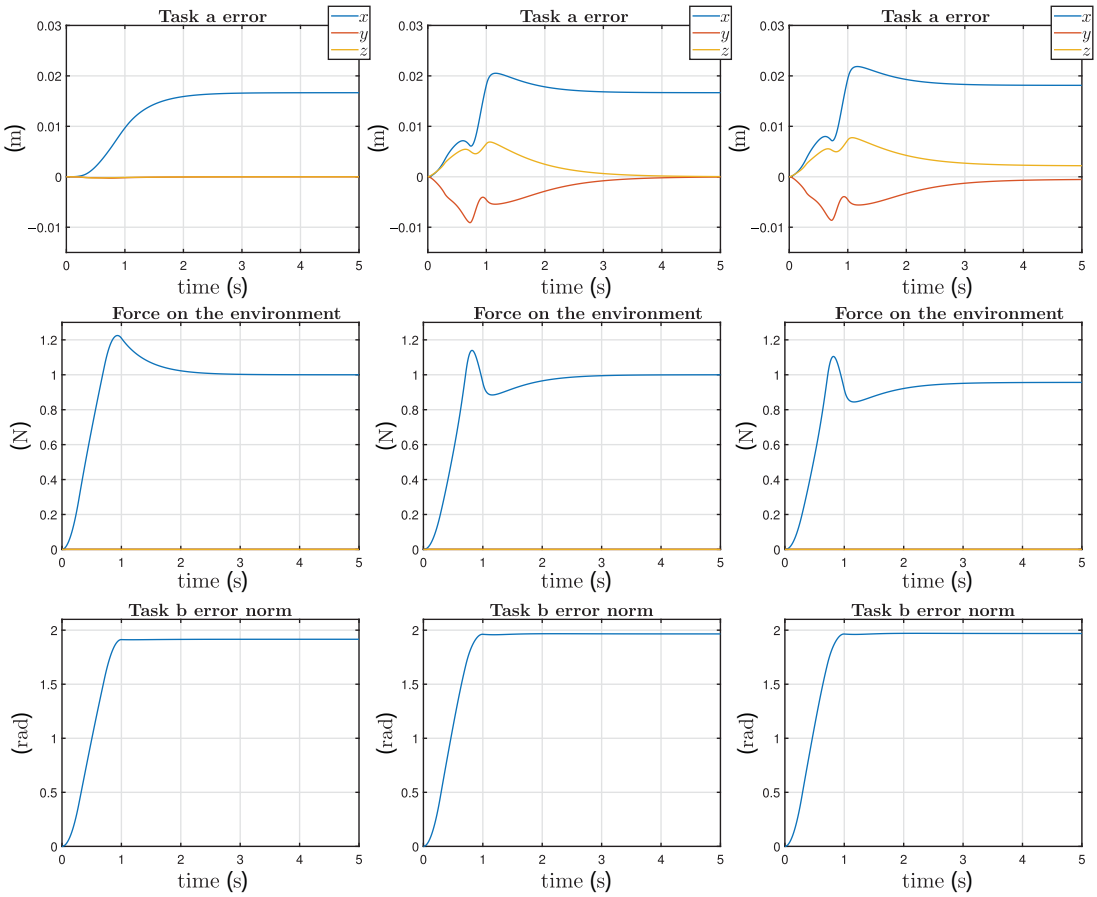


Fig. 3. Case studies 7–9. Left plots: perfect compensation of inertial and nonlinear terms. Center plots: imperfect knowledge of the sole inertia matrix. Right plots: imperfect compensation of both inertial and nonlinear terms.

The end-effector is asked to track a linear trajectory along the $x$-axis with a displacement of 5 cm following a trapezoidal velocity profile causing an interaction with the environment, while the secondary task is a desired position for all the seven joints intentionally in conflict with the primary task. Figure 3 shows the output of the numerical simulation in terms of task errors and force exchanged with the environment. The left plots, from top to bottom, represent the perfect compensation case (case study 7), the center plots the imperfect knowledge of the inertia matrix with perfect knowledge of $\hat{\boldsymbol{n}}$ (case study 8) and finally, the right plots the uncertain knowledge of the whole dynamics (case study 9). It can be appreciated that uncertainty in the knowledge of the inertia terms affects the transient, that is, the robot behavior in terms of the assigned impedance. On the other hand, as seen above, the use of a wrong null-space projector $\overline{\hat{\boldsymbol{N}}}_a$ does not couple the primary error dynamics with the secondary one, chosen conflicting in this simulation, at least at steady state. In fact, given the environment stiffness of Eq. (34), by comparing the steady-state forces reported in the middle plots with the steady-state displacements of the end effector reported in the top plots, it can be appreciated that the desired stiffness is achieved along the constrained direction of the operational space, except in the case when the gravity is not perfectly compensated (plots on the right); this happens despite the use of the wrong projector. On the other hand, the results in the middle plots confirm that the use of an uncertain inertia matrix influences the transient, as expected.

## 6. Conclusions

This paper investigates the effect of model uncertainty in the implementation of operational space task-priority control algorithms. Interestingly enough, the steady-state error noticed in the primary task is not caused by the wrong compensation of the inertial parameters even in combination with a secondary task error, but by the sole uncertain gravity terms, that is, a wrong knowledge of the first moment of inertia. Wrong compensation of the inertial terms do affect the transient in all the tasks

https://doi.org/10.1017/S0263574720001411 Published online by Cambridge University Press

and, obviously, also when an impedance controller in one of the tasks. Future research will concern a more thorough comparison of the impedance degradation in case of uncertainty, stability analysis and comparison with IK-based task-priority approaches.

## References


1. G. Antonelli, "Stability analysis for prioritized closed-loop inverse kinematic algorithms for redundant robotic systems," *IEEE Trans. Robot.* **25**(5), 985–994 (2009).
2. G. Antonelli, P. Di Lillo and C. Natale, "Modeling Errors Analysis in Inverse Dynamics Approaches within a Task-Priority Framework," *2018 IEEE Conference on Control Technology and Applications*, Copenhagen, Denmark (2018) pp. 553–558.
3. M. Bjerkeng, P. Falco, C. Natale and K. Y. Pettersen, "Discrete-Time Stability Analysis of a Control Architecture for Heterogeneous Robotic Systems," *Proceedings of the 2013 IEEE/RSJ International Conference on Intelligent Robots and Systems*, Tokyo (2013) pp. 4778–4783.
4. M. Bjerkeng, P. Falco, C. Natale and K. Y. Pettersen, "Stability analysis of a hierarchical architecture for discrete-time sensor-based control of robotic systems," *IEEE Trans. Robot.* **30**(3), 745–753 (2014).
5. A. Dietrich and C. Ott, "Hierarchical impedance-based tracking control of kinematically redundant robots," *IEEE Trans. Robot.* **36**(1), 204–221 (2020).
6. A. Dietrich, C. Ott and J. Park, "The hierarchical operational space formulation: Stability analysis for the regulation case," *IEEE Robot. Autom. Lett.* **3**(2), 1120–1127 (2018).
7. O. Khatib, "A unified approach for motion and force control of robot manipulators: The operational space formulation," *IEEE J. Robot. Autom.* **3**(1), 43–53 (1987).
8. O. Khatib, L. Sentis, J. Park and J. Warren, "Whole-body dynamic behavior and control of human-like robots," *Int. J. Humanoid Robot.* **1**(1), 29–43 (2004).
9. J. Lee, P. H. Chang and R. S. Jamisola, "Relative Task Prioritization for Dual-Arm with Multiple, Conflicting Tasks: Derivation and Experiments," *2013 IEEE International Conference on Robotics and Automation (ICRA)*, Karlsruhe, Germany (IEEE, 2013) pp. 1928–1933.
10. S. Moe, G. Antonelli, A. Teel, K. Pettersen and J. Schrimpf, "Set-based tasks within the singularity-robust multiple task-priority inverse kinematics framework: General formulation, stability analysis and experimental results," *Front. Robot. AI* **3**, 16 (2016).
11. S. Moe, A. Teel, G. Antonelli and K. Pettersen, "Stability Analysis for Set-Based Control within the Singularity-Robust Multiple Task-Priority Inverse Kinematics Framework," *54th IEEE Conference on Decision and Control and 8th European Control Conference*, Osaka, Japan (2015) pp. 171–178.
12. J. Nakanishi, R. Cory, M. Mistry, J. Peters and S. Schaal, "Comparative Experiments on Task Space Control with Redundancy Resolution," *Proceedings 2005 IEEE/RSJ International Conference on Intelligent Robots and Systems*, Edmonton, CA (2005) pp. 3901–3908.
13. J. Nakanishi, R. Cory, M. Mistry, J. Peters and S. Schaal, "Operational space control: A theoretical and empirical comparison," *Int. J. Robot. Res.* **27**(6), 737–757 (2008).
14. C. Ott, A. Dietrich and A. Albu-Schäffer, "Prioritized multi-task compliance control of redundant manipulators," *Automatica* **53**(1), 416–423 (2015).
15. J. Peters, M. Mistry, F. Udwadia, J. Nakanishi and S. Schaal, "A unifying methodology for robot control with redundant DOFs," *Auto. Robots* **24**(1), 1–12 (2008).
16. N. Roy, P. Newman and S. Srinivasa, *Experiments with Balancing on Irregular Terrains Using the Dreamer Mobile Humanoid Robot* (MITP, 2013).
17. H. Sadeghian, L. Villani, M. Keshmiri and B. Siciliano, "Dynamic multi-priority control in redundant robotic systems," *Robotica* **31**(7), 1155–1167 (2013).
18. L. Sentis, Synthesis and Control of Whole-Body Behaviors in Humanoid Systems *Ph.D. Thesis* (Stanford University, USA, 2007).
19. L. Sentis and O. Khatib, "Prioritized Multi-objective Dynamics and Control of Robots in Human Environments," *2004 4th IEEE/RAS International Conference on Humanoid Robots* (2004).
20. L. Sentis and O. Khatib, "A Whole-Body Control Framework for Humanoids Operating in Human Environments," *Proceedings 2006 IEEE International Conference on Robotics and Automation, 2006. ICRA 2006* (IEEE, 2006) pp. 2641–2648.
21. L. Sentis, J. Petersen and R. Philippsen, "Implementation and stability analysis of prioritized whole-body compliant controllers on a wheeled humanoid robot in uneven terrains," *Auto. Robots* **35**(4), 301–319 (2013).
22. B. Siciliano, L. Sciavicco, L. Villani and G. Oriolo, *Robotics: Modelling, Planning and Control* (Springer Verlag, Germany, 2009).
23. C. D. Sousa and R. Cortesão, "Inertia tensor properties in robot dynamics identification: A linear matrix inequality approach," *IEEE/ASME Trans. Mech.* **24**(1), 406–411 (2019).
24. T. Valency and M. Zacksenhouse, "Accuracy/robustness dilemma in impedance control," *J. Dyn. Syst. Meas. control* **125**(3), 310–319 (2003).


https://doi.org/10.1017/S0263574720001411 Published online by Cambridge University Press